Supporting Information

fM-aM Detection of SARS-CoV-2 Antigen by Advanced Lateral Flow Immunoassay Based on Gold Nanospheres

Yilin Liu[1], Li Zhan[1], Jesse W. Shen[1], Bàrbara Baro[2], Andrea Alemany[3,5], James Sackrison[4], Oriol Mitjà[3,5,6], John C. Bischof[1,7,*]

[1] Department of Mechanical Engineering, University of Minnesota, Minneapolis, MN 55455, USA

[2] ISGlobal, Hospital Clínic, Universitat de Barcelona, Barcelona, 08036, Spain

[3] Fight AIDS and Infectious Diseases Foundation, Badalona, 08916, Spain

[4] 3984 Hunters Hill Way, Minnetonka, MN 55345, USA

[5] Hospital Universitari Germans Trias i Pujol, Badalona, 08916, Spain

[6] Lihir Medical Centre – International SOS, Lihir Island, New Ireland, 633, Papua New Guinea

[7] Department of Biomedical Engineering, University of Minnesota, Minneapolis, MN 55455, USA

Email of the corresponding author: bischof@umn.edu

S1. Characterization of TCA's fast scanning algorithm

The fast-scanning algorithm was characterized by scanning calibration LFAs and comparison with the discrete reading algorithm used in our previous publications.[1–6] Test lines of calibration LFAs were dispensed with different concentrations of gold nanospheres (GNSs, ~100 nm in diameter) in 65% glycerol solution by a 3D printer.[4] Before printing, the GNS concentrations were characterized as the optical density (OD) at the absorbance peak absorbance for 1 cm pathlength of light through their aqueous solutions. After printing, the membrane was dried overnight and assembled to attach conjugated and wicking pads before being cut into 3 mm wide strips. Different TCA reading algorithms were used to scan these test lines.

S2. Thermal Signals of Commercial SARS-CoV-2 Lateral Flow Immunoassays (LFAs)

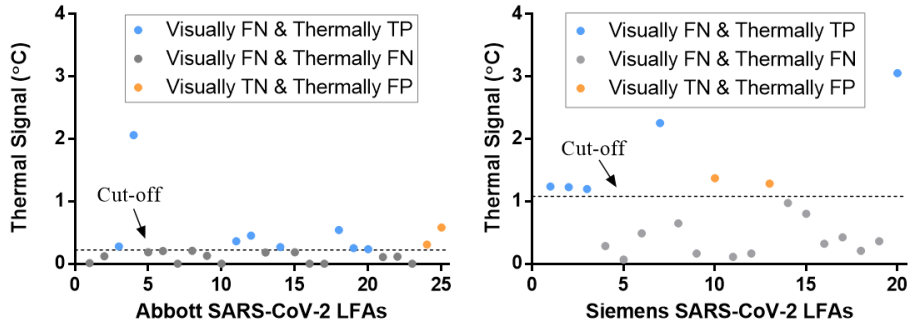

Figure S1. Thermal signals of some Abbott and Siemens SARS-CoV-2 lateral flow immunoassays (LFAs) with either visually or thermally false readout. TP: true positive; FN: false negative; FP: false positive.

S3. Images of the mouse IgG and advanced SARS-CoV-2 LFAs

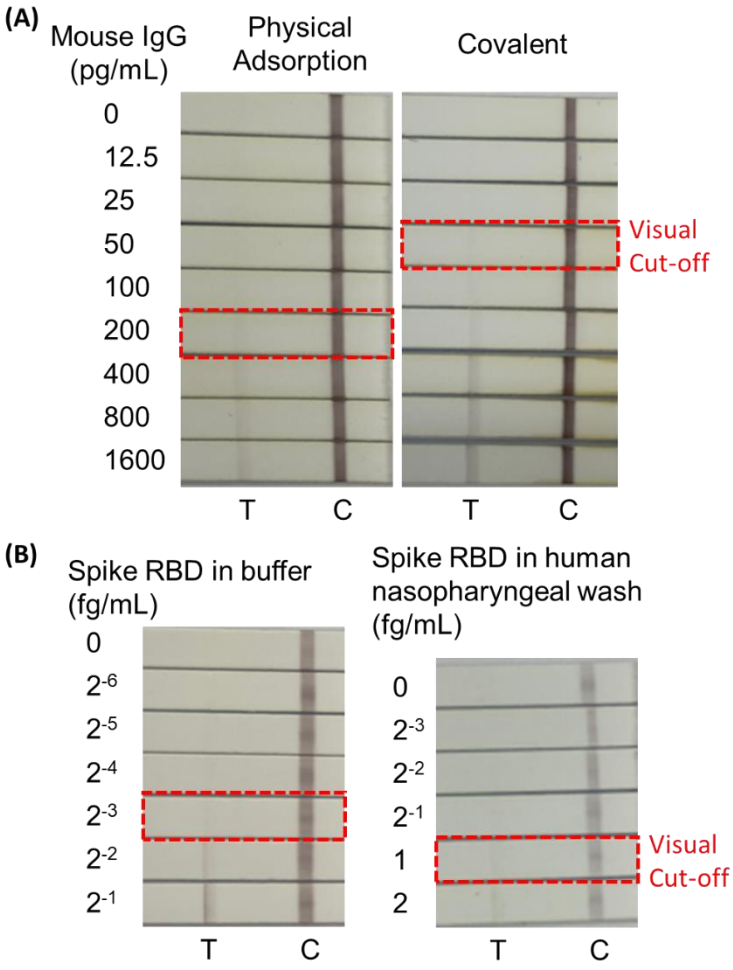

Figure S2. Images of lateral flow immunoassay strip samples. (A) Detecting mouse IgG in buffer by using physical adsorption (left) and covalent (right) conjugation methods. (B) Detecting SARS-CoV-2 spike receptor-binding domain (RBD) protein in buffer (left) and human nasopharyngeal wash (right) solutions by covalent conjugation method. Strips indicating visual detection limits (i.e., cut-off) right after testing were marked by red dashed lines. Notes: The images of the LFA strips were taken several months after testing. The strips' color gradually changed over the long time of storage after testing.

S4. Characterization of antigen-binding sites from GNS conjugates.

S4.1: Synthesizing R-PE-Antigen Conjugate

R-PE-antigen (*i.e.*, mouse IgG) conjugates were synthesized with a disulfide crosslinking bond, which could be cleaved by DTT. To obtain sulfhydryl activated R-PE, 0.5 mL 150 mM DTT was first mixed with 1 mL 1 mg/mL Pyridyl disulfide-derivative R-PE in 1x PBS-EDTA. The mixture was then left to incubate at room temperature, followed by purification by buffer exchange (1X PBS-EDTA) in ultracentrifuge desalting spin columns (87767, Thermo Fisher). Concurrently, pyridyldithiol-activated antigen was produced by mixing 12.5 uL 20 mM SPDP in dimethyl sulfoxide with 0.5 mL 1 mg/mL mouse IgG antigen (I5381, Sigma-Aldrich) in 1X PBS-EDTA. The mixture was rotated for 60 min at room temperature, followed by the same purification method as above. Finally, the RPE-antigen conjugates were synthesized by mixing the above two protein products (*i.e.*, sulfhydryl activated R-PE and pyridyldithiol-activated antigen) at equal mass concentration with rotation incubation at room temperature for 18 h. The final protein conjugates were purified by a filtration unit (0291054, Cole-Parmer) with a 200 kDa molecular weight cutoff (MWCO).

S4.2: Availability Characterized by R-PE-antigen conjugates

To characterize the availability of binding sites from GNS conjugates, the binding sites were first labeled with R-PEs through antigen-antibody binding and then quantified by fluorescence test of the released R-PEs cleaved from the GNS-antibody-antigen-RPE complexes, as shown in Figure 5D. Specifically, two types of GNS conjugates were prepared by either covalent or physical adsorption conjugation methods to link anti-mouse IgG antibodies (M8642, Sigma-Aldrich) with controlled antibody addition (*i.e.*, 5 μg antibody per mL stock GNS). The GNS conjugates were centrifuged twice and resuspended into a binding buffer (pH 8.5, 10 mM Tris buffer, 0.5% BSA) at about half GNS stock concentration. In each 0.5 mL GNS conjugate solution, 5 μL (0.25 mg/mL) R-PE-antigen conjugate was added. The mixture was rotated in the dark overnight at 4 ℃. Next, the GNS-antibody-antigen-RPE complex was collected from the solution by centrifugation and its supernatant was measured by fluorescence test to calculate excess antigen conjugates (F_{excess}). The GNS complex pellet was resuspended in a 10 mM phosphate buffer (pH=7) with 50 mM DTT, followed by rotation for 2 h at room temperature to cleave the disulfide bond and release R-Pes. Once the reaction was completed, the samples were centrifuged to obtain the supernatant with released R-PEs for fluorescence test, whose intensity indicated the availability of active binding sites from GNS conjugates (F_{bind}). To preclude GNS's interference with the fluorescence signal, all supernatants were ultracentrifuged once more to remove trace amounts of GNSs. The fluorescence was measured by a 96-well plate reader (Gemini EM, Molecular Devices) with 200 μL supernatant per well and excitation and emission wavelengths of 488 nm and 570 nm, respectively. The higher fluorescent intensity indicated a higher concentration of R-PE, whose calibration curve is shown in Figure S3. F_{bind} was normalized by the GNS concentration ratio (~1.15) between the two conjugation methods, pre-measured by spectrum before the addition of RPE-antigen conjugates. Normalized binding signal (F'_{bind}) and RPE-antigen consumption rate ($\frac{F'_{bind}}{F_{excess}+F_{bind}}$) were thus used to compare the availability of antigen-binding sites from the two types of GNS conjugates. A dark environment was needed to store and experiment with R-PE-related samples to avoid photobleaching. The number of replicates to characterize each GNS conjugation type was 6.

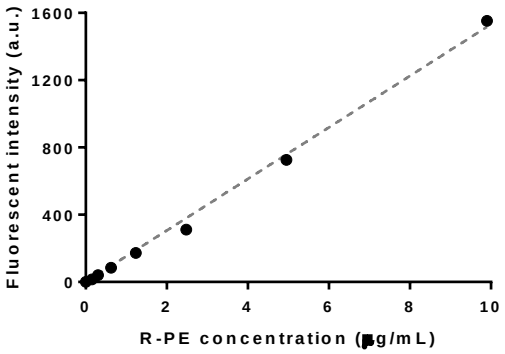

Figure S3. Calibration of the fluorescence signal of the pyridyldisulfide derivative R-phycoerythrin (R-PE) diluted in 10 mM phosphate buffer. In fluorescence test, the volume per well is 200 μL. N=3.

S5. Kinetic Analysis for LFA

According to the kinetic analysis in the previous perspective[7], most LFAs are reaction-limited, which indicates a much lower reaction rate than mass transfer rates (*i.e.*, diffusion and convection of GNSs and analytes) in LFA performance. Below, we discuss how to enhance detection sensitivity by maximizing GNS capture at a test line for samples with low analyte load from the perspective of reaction kinetics.

The amount of GNS captured at a test line by specific binding (SB) was determined by two sets of reactions:[8]

$$\begin{cases} \mathrm{P} + \mathrm{A} \rightleftharpoons \mathrm{PA} & \text{(S1)} \\ \mathrm{PA} + \mathrm{R} \rightleftharpoons \mathrm{PAR} & \text{(S2)} \end{cases}$$

and

$$\begin{cases} \mathrm{A} + \mathrm{R} \rightleftharpoons \mathrm{AR} & \text{(S3)} \\ \mathrm{P} + \mathrm{AR} \rightleftharpoons \mathrm{PAR} & \text{(S4)} \end{cases}$$

where P, A, R represented the active binding sites from detection antibodies conjugated with GNSs, the analytes, and the active binding sites from capture antibodies (i.e., receptor) at a test line, respectively. As a note, $[P]$ was the concentration of the binding sites from detection antibodies, which accounted for the multiple detection antibodies conjugated with one GNS. The PAR indicated a sandwich binding between a GNS (conjugated with detection antibody), a target analyte, and a capture antibody, which also represented a captured GNS at a test line.

We considered the case of a very low analyte concentration (e.g. < fM) with excess sample volume ($\geq$ 130 μL in a well), which was sufficient to drive all GNSs flow through an LFA. As such, the binding sites from capture antibodies (estimated as ~0.3 mM for 2 mg/mL antibody) were sufficiently available during the whole assay and their concentration stayed nearly constant as the initial concentration (*i.e.*, $[R] \cong [R_0]$).

Assume that the association rate constants for the 4 reactions in eqn (S1-S4) were k_{a1}, k_{a2}, k_{a3}, and k_{a4} and dissociation rate constants were k_{d1}, k_{d2}, k_{d3}, and k_{d4}. We also assumed the analytes and GNSs were premixed well, that the analytes were depleted quickly by reaction with GNSs, and that its concentration reached quasi-equilibrium before flowing into the test line zone. The rationality of this quasi-equilibrium assumption for analyte concentration ($[A]$) was evaluated by estimating the dimensionless number $\theta \sim 1$, as shown below. The dimensionless number, θ, in scale analysis was calculated as

$$\theta = \frac{reaction\ rate}{convection\ rate} = \frac{\frac{1}{k_d + k_a[P]}}{\frac{L}{U}} = \frac{U}{(k_d + k_a[P])L} \tag{S5}$$

where L (~15 mm in this study) was the distance that GNSs traveled to the test line, which depended on LFA design; U was GNS's flow velocity. Usually, k_a is in the range of $10^3 \sim 10^6$ $M^{-1}s^{-1}$ and k_d is in the range of $10^{-4} \sim 10^{-2}$ s^{-1}, depending on antibody affinity properties.[9] In this study, k_a and k_d were estimated as $\sim 10^6$ $M^{-1}s^{-1}$ and 10^{-2} s^{-1}, considering the high affinity of the selected Hytest antibody pair. The estimated active binding sites on GNSs' surface, $[P]$, was $\sim 10^{-8}$ M, based on the estimation of $\sim 10^9$ GNSs per LFA, releasing time of 30 min, and each GNS being loaded with ~200 oriented antibodies with 2 binding sites per antibody.[4] For most of the assay time, the liquid flow was driven by the absorption of the wicking pad. The large GNSs showed a smaller flow rate than liquid due to strong inertia. From our previous study,[4] $U \cong 0.18$ mm/s. Thus, θ was ~1 for the P+A reaction before reaching a test line in this study, indicating the rationality for the quasi-equilibrium assumption.

According to Qian et al.,[8] the quasi-equilibrium concentrations of $[PA_e]$ and [PAR] were

$$[PA_e] = \frac{1}{2}\left([\mathrm{A_0}] + [P] + \frac{k_{d1}}{k_{a1}} - \sqrt{\left([\mathrm{A_0}] + [P] + \frac{k_{d1}}{k_{a1}} \right)^2 - 4[\mathrm{A_0}][P]} \right) \tag{S6}$$

$$[PAR] = \frac{k_{a3}k_{d2}[\mathrm{R_0}][PA_e]}{k_{d2}(k_{d3} + k_{a3}[PA_e]) + k_{a2}k_{d3}[A_e]} \tag{S7}$$

where $[A_e] = [A_0] - [PA_e]$.

During the assay, $[PA_e]$, $[P]$, and $[PAR]$ were time-dependent, since the GNS concentration released from the conjugate pad gradually decreased while the analyte concentration fed from the sample in a well was constant at $[A_0]$. The accumulated GNSs captured at a test line during an assay were

$$accumulated\ PAR = \sum [PAR]\delta V \tag{S8}$$

where δV was the small liquid volume flowing through the test line. Here,

$$\delta V = \dot{Q}\,\delta t = A_{mem} U \delta t \tag{S9}$$

where $\dot{Q}$ was flow rate, δt was a small time interval, and A_{mem} was the cross section area of the capillary flow through LFA.

For simplified analysis, the association and dissociation reaction constants were scaled as $k_{a1} \sim k_{a2} \sim k_{a3} \sim k_{a4} \sim k_a$ and $k_{d1} \sim k_{d2} \sim k_{d3} \sim k_{d4} \sim k_d$. Then, eqn (S7) became

$$[PAR] \cong \frac{[R_0][PA_e]}{\frac{k_d}{k_a} + [A_0]} \tag{S10}$$

Thus, accumulated GNS at a test line became

$$accumulated\ PAR \cong \frac{[R_0]}{\frac{k_d}{k_a} + [A_0]} \int_0^T [PA_e]\dot{Q}\, dt \tag{S11}$$

where T was the total assay time, and $\int_0^T [P]\, dt$ equaled the total input amount of antigen-binding sites from GNSs.

The assay could be roughly split into two stages, depending on the concentration difference between $[P]$ and $[A]$. During the first stage (from $0\sim T_1$), $[P_1] \gg [A_0]$, which featured the initial flow of GNSs through membrane with sufficient $[P]$. During the second stage (from $T_1\sim T$), $[P_2] \sim or < [A_0]$, when $[P]$ got depleted near the end of an assay. Eqn (S11) could be then re-written as

$$accumulated\ PAR \cong \frac{[R_0]}{\frac{k_d}{k_a} + [A_0]} \left(\int_0^{T_1} [PA_e]_1\, \dot{Q} dt + \int_{T_1}^{T} [PA_e]_2\, \dot{Q} dt \right) \tag{S12}$$

During the first releasing stage ($[P_1] \gg [A_0]$), the well premixed GNSs and analyte could achieve quasi-equilibrium rapidly before entering the test line zone. At quasi-equilibrium,

$$k_a[P_1][A_e]_1 = k_d[PA_e]_1 \tag{S13}$$

Since $[A_e]_1 = [A_0] - [PA_e]_1$, $[PA_e]_1$ became

$$[PA_e]_1 = \frac{k_a[P_1][A_0]}{k_a[P_1] + k_d} \tag{S14}$$

During the second releasing stage (from $T_1\sim T$), the formation rate of $[PA]_2$ ($= k_a[P_2][A_0] \sim k_a[A_0]^2$) got much smaller. The assumption of achieving equilibrium $[PA_e]$ broke down and $[PA]$ gradually became much lower than $[A_0]$. Thus, during this stage, the GNS capture rate also decreased quickly, and was much smaller than during the first stage (from $0\sim T_1$). Therefore, eqn (S12) could be further simplified as

$$accumulated\ PAR \cong \frac{[R_0]}{\frac{k_d}{k_a} + [A_0]} \int_0^{T_1} \frac{k_a[P_1][A_0]}{k_a[P_1] + k_d} \dot{Q} dt \tag{S15}$$

As indicated in eqn (S15), multiple factors can be tailored to increase GNS accumulation by SB (*i.e.*, $accumulated\ PAR$) at a test line, boosting detection sensitivity. This can be directly achieved by increasing the concentration of active binding sites from capture antibodies ($[R_0]$) and screening for a high-affinity antibody pair which shows a higher association constant (k_a) and lower dissociation constant (k_d). Furthermore, the input GNS amount and its releasing format also play important roles. The duration of the first GNS-releasing stage (T_1) can be significantly increased by increasing the GNS input amount and releasing the GNSs more slowly. More GNS-analyte complexes can thus be formed before entering the test line, accumulating more captured GNSs at a test line. Note that, due to the capacity of conjugate and wicking pads and limited point-of-care testing time, there is a limit to the amount of input GNSs. Orienting detection antibodies on the GNS surface can thus be another method to increase the initial input of active binding sites from this surface (P) and to elongate the effective T_1.

In this work, the antibody pair for SARS-CoV-2 spike RBD was screened for high-affinity kinetics (high $\frac{k_a}{k_d}$). The capture antibody concentration was optimized to 2 mg/mL for a high reaction rate. We also chose larger GNSs (~120nm), which, compared to smaller GNSs, allowed a slower releasing format due to smaller diffusivity.[4] Detection antibodies were oriented on the GNS surface to enable a large input amount of active binding sites from GNSs. Typically, this RBD LFA took ~30 min to slowly release and let the large GNSs flow through the strip.

Note that, over-increasing the capture antibody amount and the GNS amount could elevate background noise due to nonspecific binding (NSB), and subsequently interfere with the small signal from SB. Signal amplification can enlarge both noise and signals, causing false positives. Fortunately, through our comprehensive assay optimization, NSB between GNS conjugates with capture antibodies and/or with membrane was extensively minimized. As such, the SARS-CoV-2 spike RBD LFA in this work can accommodate at least 2 mg/mL of capture antibody concentration and 6.4E8 GNSs (~120 nm) per strip (3 mm width) without false positives, even showing minimal background noise by TCA reading ($< 0.2℃$).

REFERENCES:

(1) Qin, Z.; Chan, W. C. W.; Boulware, D. R.; Akkin, T.; Butler, E. K.; Bischof, J. C. Significantly Improved Analytical Sensitivity of Lateral Flow Immunoassays by Using Thermal Contrast. *Angew. Chemie Int. Ed.* **2012**, *51* (18), 4358–4361.

(2) Boulware, D. R.; Rolfes, M. A.; Rajasingham, R.; von Hohenberg, M.; Qin, Z.; Taseera, K.; Schutz, C.; Kwizera, R.; Butler, E. K.; Meintjes, G.; Muzoora, C.; Bischof, J. C.; Meya, D. B. Multisite Validation of Cryptococcal Antigen Lateral Flow Assay and Quantification by Laser Thermal Contrast. *Emerg. Infect. Dis.* **2014**, *20* (1), 45–53.

(3) Wang, Y.; Qin, Z.; Boulware, D. R.; Pritt, B. S.; Sloan, L. M.; Gonzalez, I. J.; Bell, D.; Rees-Channer, R. R.; Chiodini, P.; Chan, W. C. W.; Bischof, J. C. Thermal Contrast Amplification Reader Yielding 8-Fold Analytical Improvement for Disease Detection with Lateral Flow Assays. *Anal. Chem.* **2016**, *88* (23), 11774–11782.

(4) Zhan, L.; Guo, S. Z.; Song, F.; Gong, Y.; Xu, F.; Boulware, D. R.; McAlpine, M. C.; Chan, W. C. W.; Bischof, J. C. The Role of Nanoparticle Design in Determining Analytical Performance of Lateral Flow Immunoassays. *Nano Lett.* **2017**, *17* (12), 7207–7212.

(5) Zhan, L.; Granade, T.; Liu, Y.; Wei, X.; Youngpairoj, A.; Sullivan, V.; Johnson, J.; Bischof, J. Development and Optimization of Thermal Contrast Amplification Lateral Flow Immunoassays for Ultrasensitive HIV P24 Protein Detection. *Microsystems Nanoeng.* **2020**, *6* (1), 54.

(6) Liu, Y.; Zhan, L.; Wang, Y.; Kangas, J.; Larkin, D.; Boulware, D. R.; Bischof, J. C. Improved Influenza Diagnostics through Thermal Contrast Amplification. *Diagnostics* **2021**, *11* (3), 462.

(7) Liu, Y.; Zhan, L.; Qin, Z.; Sackrison, J.; Bischof, J. C. Ultrasensitive and Highly Specific Lateral Flow Assays for Point-of-Care Diagnosis. *ACS Nano*. February 19, 2021, pp 3593–3611.

(8) Qian, S.; Bau, H. H. A Mathematical Model of Lateral Flow Bioreactions Applied to Sandwich Assays. *Anal. Biochem.* **2003**, *322* (1), 89–98.

(9) Karlsson, R.; Michaelsson, A.; Mattsson, L. Kinetic Analysis of Monoclonal Antibody-Antigen Interactions with a New Biosensor Based Analytical System. *J. Immunol. Methods* **1991**, *145* (1–2), 229–240.